Fire Safety Journal 106 (2019) 114–123

Contents lists available at ScienceDirect

Fire Safety Journal

journal homepage: www.elsevier.com/locate/firesaf

Quantification of cross-wind effect on temperature elevation in the downwind region of fire sources

Keisuke Himoto

National Institute for Land and Infrastructure Managemen, Tachihara 1, Tsukuba, Ibaraki, 305-0802, Japan

ARTICLE INFO

Keywords:
Wind-blown fire plume
Cross-wind
Temperature elevation
Wind tunnel experiment

ABSTRACT

The effect of cross-wind on the temperature elevation in the downwind region of square diffusion burners was investigated in wind tunnel experiments. The experimental parameters were the side length of the square diffusion burner (0.4–1.2 m), the heat release rate (38.3–345 kW), and the inflow velocity of the cross-wind (0.59–1.49 m/s). To describe the transition of the half-width of the cross section, the temperature elevation, and the velocity of fire plumes along the trajectory, a similarity model was derived by dimensional analysis. This model is equivalent to that in a quiescent environment, with the cross-wind effect embodied in the distance along the trajectory. Therefore, the derived model reasonably correlated the half-width of the cross section with the temperature elevation. It also obtained the measured temperature elevation at ground level (0.02 m above the floor) downwind of the fire sources. In this evaluation, the correlation between the measured and computed data points was improved by introducing a virtual source that considered both the fire source size and the cross-wind velocity effects.

1. Introduction

Quantifying the cross-wind effect on the behavior of flames and fire plumes is important for combatting large outdoor fires such as urban and wildland fires. Cross-winds tilt and extend the flames, accelerating the fire spread by strengthening the heat transfer to other combustibles in the downwind. Relatively far downwind of the fire source, wind-blown fire plumes envelop a wide areal range. Even when the temperature elevation is mild and cannot ignite the combustibles, wind-blown plumes hamper the firefighting activity and evacuation of residents.

Cross-wind effects on flames and fire plumes have gathered considerable attention; especially, researchers focused on the rate of fire spread between combustibles by investigating the behavior of flames and fire plumes within the vicinity of a fire source [1–10]. However, the behavior of fire plumes far downwind of the fire sources has not been completely investigated. Among the existing studies of long-range fire plumes, Yokoi [11] and Saga [12] independently investigated the tilt angle and temperature elevation induced by wind-blown fire plumes in wind tunnel experiments. They assumed linear fire sources of 0.85 m × 0.01 m (range of Froude number Fr = 2.43–6.36) and 0.5 m × 0.05 m–0.2 m (Fr = 0.52–4.36), respectively. They analyzed the experimental result on a two-dimensional plume model that ignored the distribution perpendicular to the cross-wind [11,12]. Hayashi et al. measured the temperature elevation downwind of two separate diffusion burners with a side length of 0.3 m in a wind tunnel experiment (Fr = 0.583–1.75). They generalized the plume model of Saga by collecting the heat release rates of the two diffusion burners into one representative value [13]. Oka et al. approximated the fire plume trajectory downwind of a circular diffusion burner of diameter 0.2 m by a logistic curve fitting (Fr = 0.448–1.59) [14]. Later, they measured and empirically correlated the velocities along trajectories through bidirectional pitot tubes downwind of fire sources with different geometries (square diffusion burners with side lengths of 0.5 m and 1.0 m, and rectangular diffusion burners with dimensions of 0.1 m × 0.3 m and 0.1 m × 0.5 m, Fr = 0.417–0.994) [15]. Although the results of these studies provide valuable insight into the behavior of wind-blown fire plumes, the experimental fire sources were relatively small. Moreover, as generating low-velocity cross-wind in a reproducible and stable manner is technically difficult in a wind tunnel experiment, the cross-wind velocities in the previous experiments were large relative to the fire-source dimensions. In fact, part of the existing plume models assumes strong cross-wind effect relative to buoyancy that the fire plume trajectory is almost parallel to the ground, and that the velocity is equivalent to the cross-wind velocity under strong wind conditions [12,13].

In the present study, the effect of cross-wind on the temperature elevation downwind of relatively large fire sources (square diffusion

E-mail address: himoto-k92ta@mlit.go.jp.

https://doi.org/10.1016/j.firesaf.2019.04.010
Received 13 January 2019; Received in revised form 17 April 2019; Accepted 18 April 2019
Available online 24 April 2019
0379-7112/

Nomenclature

Alphabet

B^*	Dimensionless cross-sectional half-width of the fire plume [−]
b	Cross-sectional half-width of the fire plume [m]
c_P	Heat capacity [kJ/kgK]
D	Reference length [m]
g	Acceleration due to gravity [m/s^2]
N	Fractional contribution of cross-wind velocity on velocity along trajectory
$\dot{Q}$	Heat release rate of the fire source [kW]
s	Distance along the trajectory [m]
S^*	Dimensionless distance along the trajectory [−]
ΔT	Temperature elevation [K]
T_∞	Ambient gas temperature [K]
T^*	Dimensionless temperature elevation [−]
U	Reference velocity [m/s]
U_∞	Cross-wind velocity [m/s]
U^*	Dimensionless cross-wind velocity [−]
u	Velocity along the trajectory of the fire plume [m/s]
W	Side length of the fire source [m]
W^*	Dimensionless vertical velocity [−]
w	Vertical velocity [m/s]
X^*	Dimensionless horizontal distance from the fire source [−]
x	Horizontal distance from the fire source [m]
z	Height from the floor [m]

Greek letters

ρ	Fire plume density [kg/m^3]
ρ_∞	Ambient gas density [kg/m^3]
$\Delta\rho$	Density difference [kg/m^3]

burners with side lengths ranging from 0.4 m to 1.2 m) was investigated in a series of wind tunnel experiments under relatively mild cross-wind velocities (Fr = 0.0540–0.753). A similarity model describing the cross-sectional half-width, temperature elevation, and velocity along the trajectory of a wind-blown fire plume was then derived by dimensional analysis. In contrast to the existing plume model that assumes a strong wind effect, the velocity along the trajectory is contributed by both the buoyancy-induced upward velocity and the cross-wind velocity. The fractional contributions of each component are determined experimentally. Finally, to evaluate the human activity hazard in the event of a large outdoor fire, the ground-level temperature elevation downwind of each fire source was correlated with the result of the derived model.

2. Wind tunnel experiment

The experimental setup in the wind tunnel is schematized in Fig. 1. The wind tunnel was an open-loop boundary-layer wind tunnel, in which the inflow generated by the fan is unaffected by the heat generation from the fire source in the measurement section. The wind tunnel consisted of two consecutive measurement sections. The first measurement section was 10 m long in the wind direction, with an orthogonal cross-section of 5 m × 4 m (width × height). The second measurement section was 15 m long in the wind direction, with an orthogonal cross-section of 5 m × 14 m (width × height). In the first measurement section, a combination of a saw-edged barrier, vortex generators (spires), and surface roughness were aligned to experimentally generate a flow that has similar properties to that of the thermally neutrally stratified atmospheric boundary layer (the first measurement section was not used for measurement in the present experiment) [16–18]. In the second measurement section, a wind-blown fire plume was generated by passing the experimentally generated flow over a fire formed above a square diffusion burner. The origin of the coordinate system was the leeward end of the diffusion burner. The x, z, and s axes were aligned along the wind direction, the vertical direction, and the trajectory of the fire plumes, respectively.

The experimental conditions are summarized in Tables 1 and 2. The three experimental parameters were the side length of the burner W, the heat release rate $\dot{Q}$, and the cross-wind velocity U_∞. To accommodate the constraints of the measurement equipment, we measured the temperature elevation around the trajectory and near the floor in separate experiments (see Tables 1 and 2). Note that range of cross-wind velocities in Table 1 is the range of average cross-wind velocities of four tests with the same length of the burner W, heat release rate $\dot{Q}$ and rotation rate of the fan. The four tests were conducted under identical conditions for measuring temperature elevation ΔT around trajectories since measurement had to be interrupted for manually shifting the location of a tree of thermocouples from 0.5 m to 2.0 m downwind of the diffusion burner at 0.5-m intervals. Although rotation rate of the fan was maintained the same, there were slight variation in the generated cross-wind velocities between the four tests (Table 1). On the other hand, temperature elevation ΔT near the floor was measured in one consecutive test since fixed alignment of thermocouples were used for the measurement. Thus, there are one average cross-wind velocity for one test condition (Table 2). All test cases listed in Tables 1 and 2 were recorded for 5 min, and the data of the final 3 min were

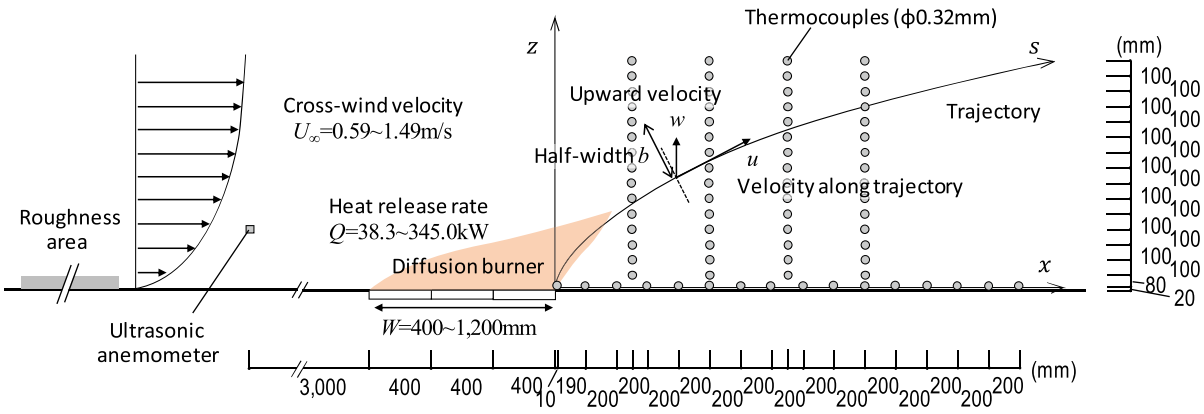

Fig. 1. Schematic of experimental setup in the wind tunnel.

Table 1
Experimental conditions of temperature elevation measurements along the trajectories.

Side length of fire source W (m)	Heat release rate $\dot{Q}$ (kW)	Cross-wind velocity U_∞ (m/s)
0.4	38.3	0.59–0.66, 0.94–1.05, 1.43–1.44
0.4	63.9	0.70–0.79, 1.06–1.12, 1.42–1.44
0.4	89.4	0.73–0.78, 1.06–1.10, 1.40–1.44

Table 2
Experimental conditions of temperature elevation measurements at 0.02 m above the floor.

Side length of fire source W (m)	Heat release rate $\dot{Q}$ (kW)	Cross-wind velocity U_∞ (m/s)
0.4	38.3	0.72, 1.03, 1.47
0.4	63.9	0.67, 1.03, 1.45
0.4	89.4	0.72, 1.02. 1.49
0.8	155.3	0.82, 1.12, 1.46
0.8	255.6	0.76, 1.11, 1.47
1.2	345.0	0.82, 1.17, 1.48

reserved for analysis.

2.1. Fire source

The square diffusion burner comprised nine component burners arrayed in a (3 × 3) square lattice, with the rows and columns corresponding to the wind and perpendicular directions, respectively. The side length of each component burner was 0.4 m, and the side length W of the fire source was varied as 0.4 m, 0.8 m, and 1.2 m by controlling the quantity of fuel fed to the component burners. The surfaces of all component burners were tightly contacted with the floor level, and wrapped with a 25 mm-thick ceramic fiber blanket to ensure a uniform flame formation over the surface under cross-wind conditions. The heat release rate $\dot{Q}$of the fire source was obtained by multiplying the heat of combustion of the fuel by the volume supply rate measured by an ultrasonic flowmeter installed in the middle of the piping. In the present experiment, the fuel was city gas, and $\dot{Q}$ was controlled as 38.3, 63.9, 89.4, 155.3, 155.3, 255.6, and 345.0 kW.

2.2. Cross-wind

In the absence of fire sources, the vertical profile of the generated inflow velocity (x- and z-axial components) was measured by a hot wire anemometer (X-type probe, φ5μ tungsten) placed at 3 m windward from the diffusion burner. The anemometer was raised from 0.025 m to 2.0 m above the floor by a transverse device, collecting measurements at twenty five points. The sampling frequency was 1000 Hz, cut off at 400 Hz by a low-pass filter. At each measurement point, the inflow velocity was obtained as the ensemble average of 10 inflow-velocity measurements, each of 30 s duration. The profile of the generated inflow velocity (see Fig. 2) constitutes the means and standard deviations of the mainstream component U and the vertical component W. The reference mainstream velocity at 2.0 m above the floor, denoted by U_0, was approximately 2 m/s. The vertical profile of the mainstream component of natural wind is often approximated as a power law of the form

$$U/U_0 = (z/z_0)^\alpha \quad (1)$$

In the present experiment, the power index α of the approximated vertical profile of U was set to 0.2, which typifies α in low-rise residential areas [19,20].

When the fire sources were installed, the inflow velocity U_∞ was measured by an ultrasonic anemometer (measurement resolution: 0.01 m, nominal accuracy: ± 2% at 12 m/s) placed 3 m windward from the diffusion burner and 0.4 m above the floor. The measurement interval was 0.25 s.

2.3. Measurement of temperature elevation

The temperature elevation ΔT downwind of the fire sources was measured by thermocouples (K-type φ0.32 mm). Around the trajectory, the ΔT was measured by a tree of fifteen thermocouples vertically aligned from 0.1 m to 1.5 m above the floor at 0.1-m intervals. The thermocouple tree was manually shifted from 0.5 m to 2.0 m downwind of the diffusion burner at 0.5-m intervals. At 0.02 m above the floor, ΔT was measured by sixteen thermocouples horizontally aligned from 0.01 m to 3.0 m from the leeward edge of the diffusion burner. The first and second thermocouples were placed at 0.01 m and 0.2 m from the diffusion burner, respectively. Thereafter, the thermocouples were placed at 0.2-m intervals. All thermocouples recorded the temperature in 2-s intervals. Fig. 3 shows how the temperature elevation ΔT was measured downwind of a fire source releasing heat at the rate $\dot{Q}$ = 63.9 kW. The obtained distribution shows the height changes in the maximum temperature elevation caused by the cross-wind velocity U_∞.

3. Quantification of cross-wind effect on fire plume behavior

3.1. Transition of characteristic properties along the trajectory

The measurement results were analyzed in a similarity model describing the transition of the characteristic properties along the trajectory of a fire plume. The model assumptions are listed below:

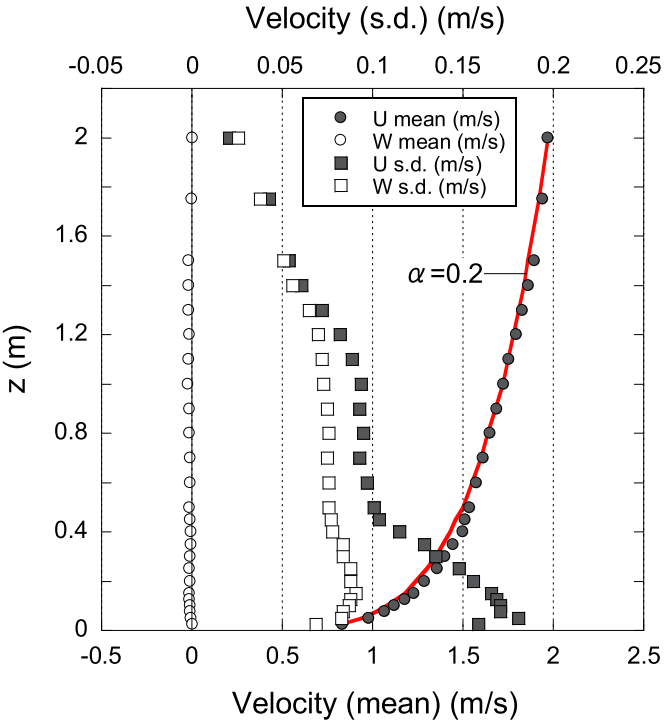

Fig. 2. Vertical profile of generated inflow velocity (reference velocity ~2 m/s).

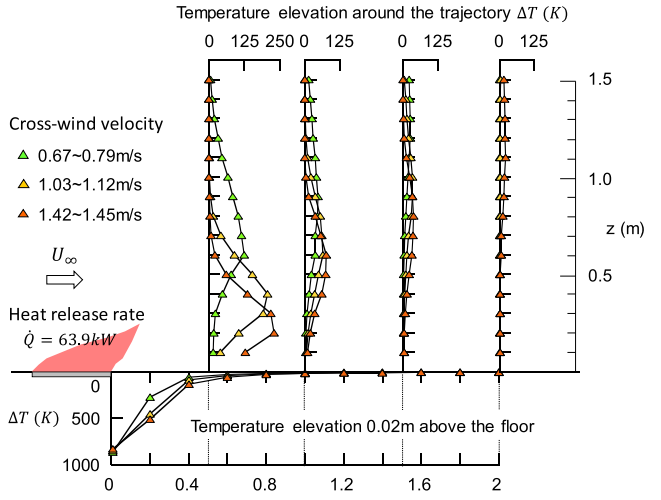

Fig. 3. Temperature elevation downwind of a fire source releasing 63.9 kW of heat.

1) The fire source geometry negligibly affects the behavior of a fire plume relatively far downwind of the fire source. Therefore, the fire source can be represented as a point source on the ground.
2) The scale and intensity of turbulence are governed mainly by the thermal instability of the fire plume, and the rate of ambient air entrainment is proportional to the vertical velocity driven by buoyancy [21].
3) The vertical momentum is predominantly driven by the buoyancy force; the viscous force can be ignored.
4) The heat loss from the wind-blown fire plume to the ground is negligible at all tilt angles.

Based on these assumptions, the conservational relationships of mass, vertical momentum and thermal energy are respectively given by

$$\rho b^2 u \propto \int \rho_\infty b w \, ds \tag{2}$$

$$\rho u w \propto \Delta\rho g s \tag{3}$$

$$\dot{Q} \propto c_P \rho b^2 u \Delta T \tag{4}$$

Here, c_P is the heat capacity of the gas, g is the gravitational acceleration, b is the cross-sectional half-width, and s and u are the distances and velocities along the trajectory, respectively. w is the vertical velocity, ρ and ρ_∞ are the gas density and ambient gas density, respectively, and $\Delta\rho$ is the density difference. Under atmospheric pressure, ρT can be considered constant and Eq. (3) reduces to

$$u w \propto \frac{\Delta T}{T_\infty} g s \tag{5}$$

where T_∞ is the ambient gas temperature.

The three conservational relationships (Eq. (2), (4), and (5)) involve four unknown characteristic parameters: the half-width of the cross-section b, the velocity along the trajectory u, the upward vertical velocity w, and the temperature elevation ΔT. Thus, these simultaneous equations must be closed by an additional model. When the cross-wind velocity U_∞ is sufficiently small, the velocity u along the trajectory can be considered equivalent to the upward velocity w of the fire flume. On the other hand, whenU_∞ is sufficiently stronger than the vertical velocity w, the velocity along the trajectory u can be considered equivalent to the cross-wind velocity U_∞. Exploiting this antipodal relationship, the velocity along the trajectory u can be approximated by

$$u \sim w^{1-N} U_\infty^N \tag{6}$$

where N is a real number between 0 and 1; the effect of the cross-wind is negligible if N is 0, and prevailing if N is 1. Thus, N can be considered as the fractional contribution of cross-wind velocity on velocity along trajectory. Substituting the velocity along the trajectory u in Eqs. (2), (4) and (5), using Eq. (6), and introducing the dimensionless parameters

$$S^* = \frac{s}{D},\ B^* = \frac{b}{D},\ W^* = \frac{w}{U},\ U^* = \frac{U_\infty}{U},\ T^* = \frac{\Delta T}{T_\infty} \tag{7}$$

Eqs. (2), (4) and (5) can be respectively transformed into the following forms:

$$B^{*2} W^{*1-N} U^{*N} \propto B^* W^* S^* \tag{8}$$

$$W^{*2-N} U^{*N} \propto \left(\frac{gD}{U^2}\right) T^* S^* \tag{9}$$

$$B^{*2} W^{*1-N} U^{*N} T^* \propto \left(\frac{\dot{Q}}{c_P \rho_\infty T_\infty D^2 U}\right) \tag{10}$$

Here, D is the reference length and U is the reference velocity. For simplicity, the fire plume density ρ in the above transformation was assumed to equal the ambient gas density ρ_∞. This is reasonable because the present study investigates the temperature elevation in the relatively far downwind region of the fire source. In the dimensionless parameters defined by Eq. (7), the reference length D and reference velocity U can be determined such that the parameters in the parentheses in Eqs. (9) and (10) become unity, namely,

$$D = \left(\frac{\dot{Q}}{c_P \rho_\infty T_\infty g^{1/2}}\right)^{2/5},\ U = g^{1/2}\left(\frac{\dot{Q}}{c_P \rho_\infty T_\infty g^{1/2}}\right)^{1/5} \tag{11}$$

To elucidate how the dimensionless characteristic parameters of the fire plume (i.e., the half-width B^*, the vertical velocity W^*, and the temperature rise T^*) are influenced by the distance along the trajectory S^* and the cross-wind velocity U^*, we conduct a dimensional analysis. To this end, the following expressions are substituted into Eqs. (8)–(10),

$$B^* = C_l (S^*)^l,\ W^* = C_m (S^*)^m,\ T^* = C_n (S^*)^n \tag{12}$$

Note that the cross-wind velocity U^* is indifferent to the distance along the trajectory S^*, i.e., $U^* \propto (S^*)^0$. The power indices l, m, n, and the coefficients, C_l, C_m, C_n can be determined as follows:

$$l = 1 - \frac{N}{3},\ m = -\frac{1}{3},\ n = \frac{N}{3} - \frac{5}{3} \tag{13}$$

$$C_l \propto (U^*)^{-N},\ C_m \propto (U^*)^0,\ C_n \propto (U^*)^N \tag{14}$$

Summarizing the above considerations, the transitions of the characteristic parameters along the trajectory under the effect of the cross-wind are given by the following dimensionless expressions:

$$B^* \propto (S^*)^{1-N/3} (U^*)^{-N} \tag{15}$$

$$W^* \propto (S^*)^{-1/3} \tag{16}$$

$$T^* \propto (S^*)^{N/3-5/3} (U^*)^N \tag{17}$$

When $N = 0$, the above relationships are equivalent to those in a quiescent environment, when the effect of the cross-wind velocity is negligible [22].

3.2. Trajectory of wind-blown fire plume

The temperature elevation caused by a wind-blown fire plume is maximized along the trajectory and decreases with distance from the trajectory. However, because the fire plume rarely travels along the ground, the trajectory must be predicted for evaluating the hazards posed to human activity in the downwind of large outdoor fires. The temperature elevation along the trajectory and the attenuation away from the trajectory are also important. Based on the arguments in the previous subsection, the trajectory of a fire plume can be obtained by solving

$$z = \int \frac{dz}{dx}dx = \int \frac{w}{U_\infty}dx \tag{18}$$

where the horizontal velocity of the fire plume is assumed equivalent to the cross-wind velocity U_∞. Using Eq. (16), the vertical velocity w of the fire plume is given by

$$w \propto g^{1/2}\left(\frac{\dot{Q}}{c_P\rho_\infty T_\infty g^{1/2}}\right)^{1/3} s^{-1/3} \tag{19}$$

If the distance along the trajectory is considered proportional to the horizontal distance from a wide-range view, i.e., $s \propto x$, we can substitute Eq. (19) into Eq. (18), obtaining

$$z \propto \frac{g^{1/2}}{U_\infty}\left(\frac{\dot{Q}}{c_P\rho_\infty T_\infty g^{1/2}}\right)^{1/3} x^{2/3} \tag{20}$$

The above equation is further nondimensionalized by incorporating the side length of the fire source W as the reference length,

$$\frac{z}{W} \propto \dot{Q}_W^{*1/3} U_W^{*-1}\left(\frac{x}{W}\right)^{2/3} \tag{21}$$

where $\dot{Q}_W^*$ and U_W^* are the dimensionless parameters respectively defined as follows,

$$\dot{Q}_W^* = \frac{\dot{Q}}{c_P\rho_\infty T_\infty g^{1/2}W^{5/2}} \text{ and } U_W^* = \frac{U_\infty}{\sqrt{gW}} \tag{22}$$

This model predicts that as the trajectory separates from the fire source, it continuously loses buoyancy by entraining ambient air. By this mechanism, it gradually becomes parallel to the cross-wind. However, the trajectory cannot converge onto a horizontal line, because the decay of upward momentum by viscous forces is not considered in the model.

4. Results and discussion

4.1. Trajectory of wind-blown fire plume

To ease the discussion in the following subsections, the trajectory model was firstly validated against the measured results. Fig. 4 displays the measured trajectory with the dimensionless height z/W along the vertical axis and the dimensionless distance $\dot{Q}_W^{*1/3}U_W^{*-1}(x/W)^{2/3}$ (estimated by expression in Eq. (21)) along the horizontal axis. The trajectory height was determined by averaging the heights at which the thermocouples recorded the maximum temperature at each measurement time. The standard deviations were also computed and are plotted as the error bars in Fig. 4. The data points are linearly distributed, indicating a proportionality relationship between the two parameters, and supporting Eq. (21) in the developed model. Setting the intercept to zero (because the trajectory starts from the origin), the regression line of these data points is given by

$$\frac{z}{W} = 0.59\dot{Q}_W^{*1/3}U_W^{*-1}\left(\frac{x}{W}\right)^{2/3} \quad (R^2 = 0.921) \tag{23}$$

Fig. 5 plots the predicted results of Eq. (23) for different heat release rates $\dot{Q}$ and cross-wind velocities U_∞, along with their standard deviations (error bars). The model captures the overall characteristic of the trajectory; that is, the effect of the cross-wind strengthens with increasing distance from the fire source, although there are discrepancies between the calculated and measured results. As mentioned in the previous section, the model underestimates the decay of the upward momentum because it disregards the viscous force. However, as the trajectories of all fire plumes remained non-parallel to the horizontal line, this limitation was not serious within the range of the present measurements. The applicability of Eq. (23) is limited to the range of the present experiment, which is $\dot{Q}_W^{*1/3}U_W^{*-1}(x/W)^{2/3} < 9.6$.

4.2. Temperature elevation along the trajectory

Fig. 6 shows the measured temperature elevations ΔT_0 along the trajectories of fire plumes with different heat release rates and cross-wind velocities. As described in the previous section, the temperature elevation along the trajectory was obtained by averaging the maximum temperature elevation recorded at each measurement time. The distance along the trajectory s was calculated as the distance connecting successive points of maximum temperature elevation along each measurement line in the wind direction (i.e. the x direction). Clearly, the temperature elevation along the trajectory is an increasing function of the heat release rate $\dot{Q}$. However, the cross-wind velocity U_∞ exerts no apparent effect, as the data points of plumes with the same $\dot{Q}$ but different U_∞ overlap.

The effect of the cross-wind velocity U^* is represented by the power index N in Eq. (17). As Eq. (17) describes the proportionality of the dimensionless temperature elevation T^* along the trajectory, it can be rearranged to separate N from the other parameters as follows:

$$T^*S^{*5/3} \propto (S^{*1/3}U^*)^N. \tag{24}$$

Fig. 7 plots $T^*S^{*5/3}$ versus $S^{*1/3}U^*$ computed from the measured values. The data points are distributed almost on a horizontal line (within a certain error). The power index N can be obtained by regressing a power function to these data points. The result was 0.035, indicating that $T^*S^{*5/3}$ is almost independent of $S^{*1/3}U^*$. However, we should not conclude a negligible effect of cross-wind velocity U^* on the dimensionless temperature rise along the trajectory T^*, as the trajectory is bent by the cross-wind. Therefore, the effect can be consolidated into the dimensionless distance S^* along the trajectory.

Assuming that the power index N is zero, the dimensionless temperature elevation T^* along the trajectory was correlated with the dimensionless distance S^* along the trajectory raised to the power of $-5/3$. The correlation is plotted in Fig. 8. The data points are almost linearly distributed and satisfy the following regression equation:

$$T^* = 2.08S^{*-5/3} \quad (R^2 = 0.964) \tag{25}$$

This expression is equivalent to that in a quiescent environment, except that the distance from the fire source is the distance along the curved trajectory in the present experiment, but the height from the fire source

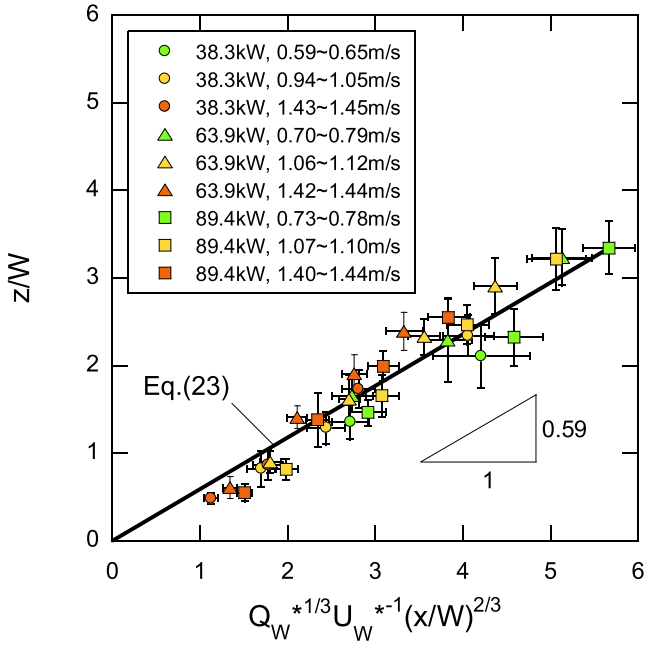

Fig. 4. Regression result of the trajectory model. The error bars are the standard deviations.

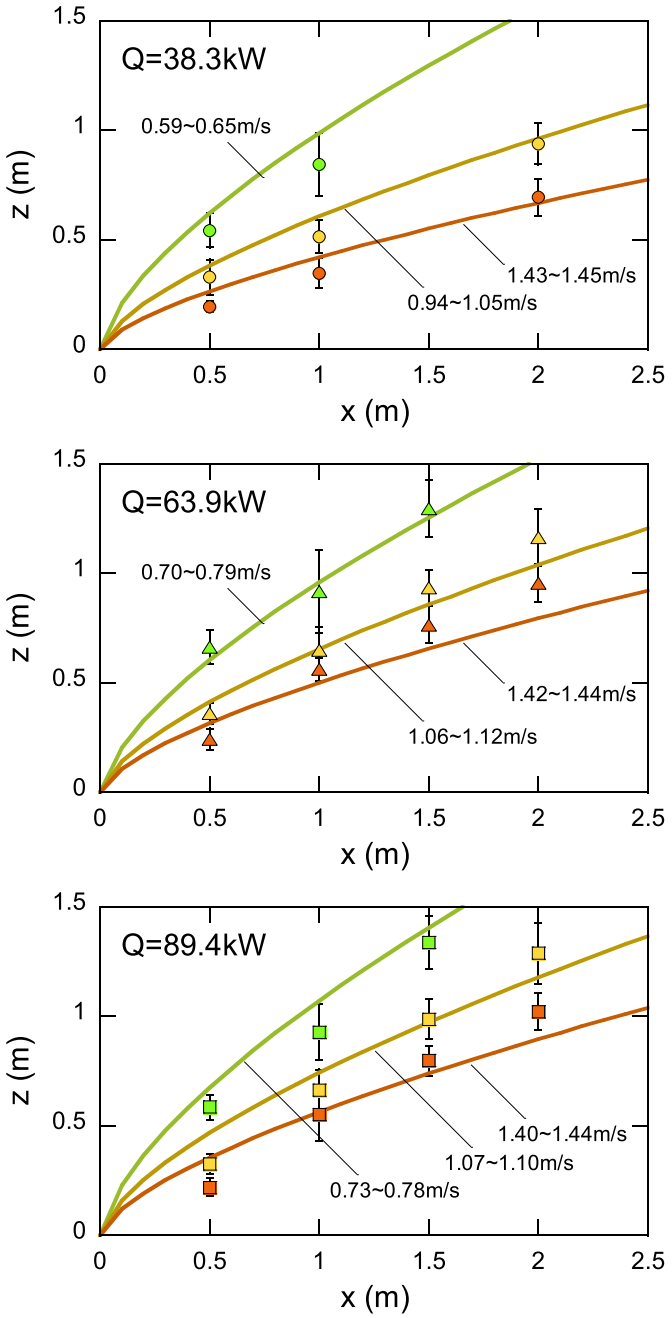

Fig. 5. Comparison of the predicted trajectories (solid lines) and measured trajectories (data points) of fire plumes with different heat release rates and cross-wind velocities.

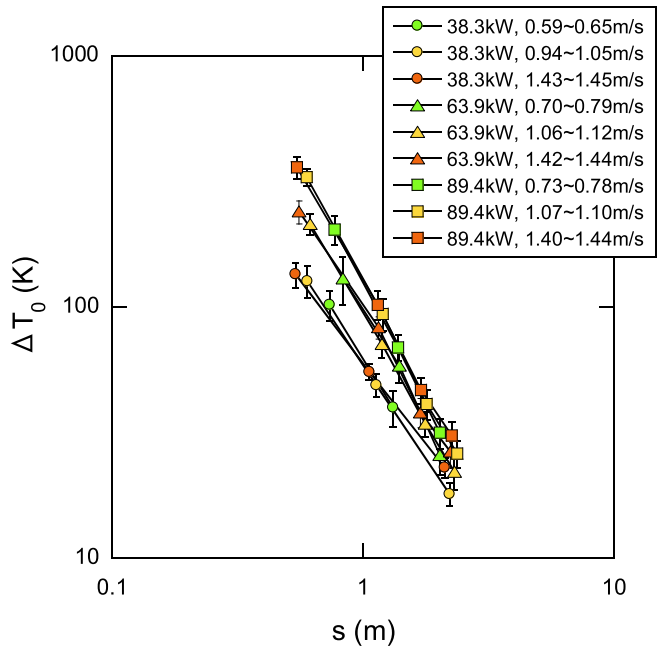

Fig. 6. Temperature elevations along the trajectories of fire plumes with different heat release rates and cross-wind velocities. Error bars are the standard deviations.

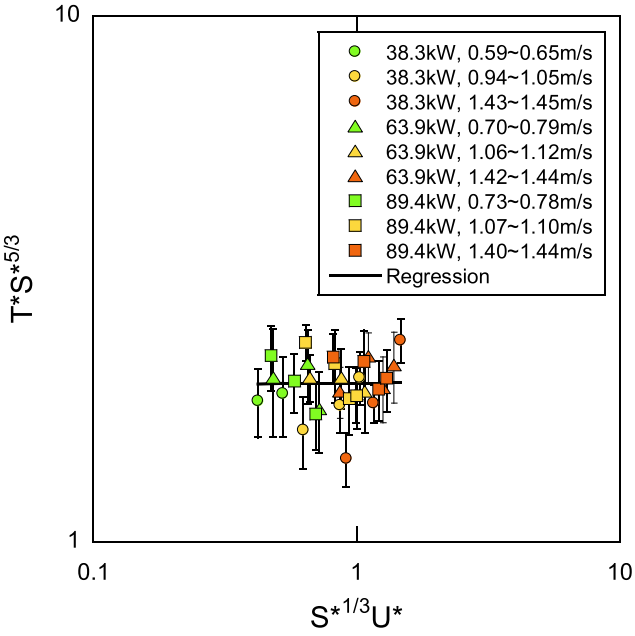

Fig. 7. Effect of cross-wind velocity on temperature elevation along the trajectory of a flame plume. Error bars are the standard deviations.

in a quiescent environment. As an example of temperature elevation in a quiescent environment, we add the result of Zukoski et al. [22] given by,

$$T^* = 9.13S^{*-5/3} \tag{26}$$

to Fig. 8. The proportionality coefficient in the present experiment was 2.08 (see Eq. (25)), substantially smaller than the value of 9.13 derived by Zukoski et al. [22]. This can be attributed to the difference in the entrainment rate of ambient air into fire plumes between the two environments; the entrainment rate is greater in the cross-wind environment than in a quiescent environment resulting in lower temperature elevation (smaller coefficient) in the cross-wind environment. Although the result of the present experiment was well correlated with the unique proportionality coefficient in the tested range of cross-wind velocities, the discrepancy between the two proportionality coefficients implies that in some range of cross-wind velocities, a behavioral transition occurs in which the proportionality trend bridges the high and low proportionalities.

4.3. Temperature elevation around the trajectory

Fig. 9 plots the temperature elevation around the trajectory ΔT(normalized by the temperature elevation along the trajectory ΔT_0) versus the separation distance from the trajectory z− z_0 (normalized by the distance along the trajectory s), in fire plumes with different heat release rates and cross-wind velocities. Although the data points vary,

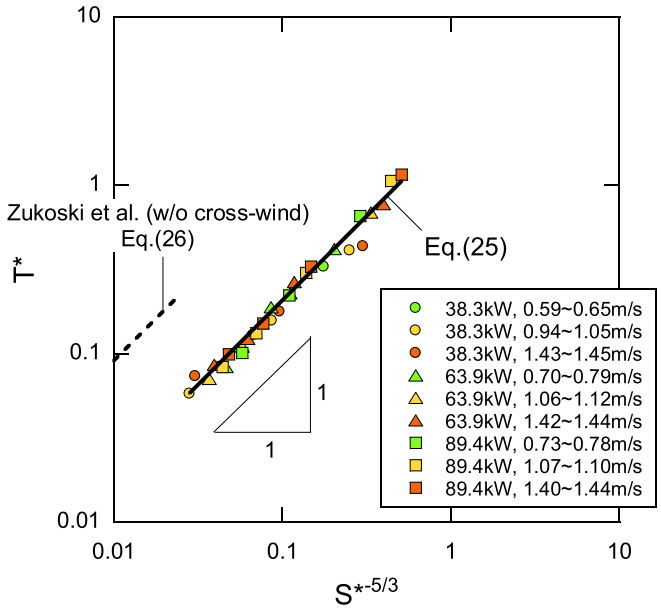

Fig. 8. Dimensionless temperature elevation along the trajectory of a flame plume.

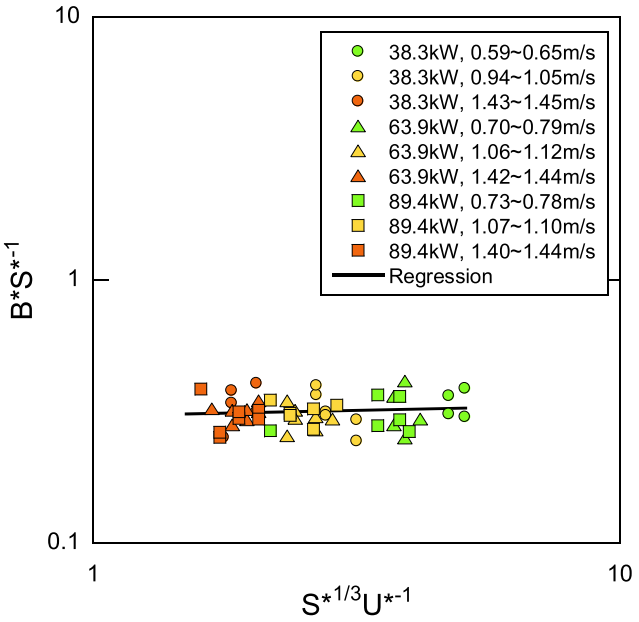

Fig. 10. Effect of cross-wind velocity on the half-width of the temperature elevation in fire plumes with different heat release rates.

especially at the lower side of the trajectory where the fire plumes are disturbed by the floor, their profiles are similar for all heat release rates $\dot{Q}$ and cross-wind velocities U_∞. This result suggests that the half-width of the cross section b is proportional to the distance along the trajectory s.

When analyzing the dimensionless temperature elevation T^*, we transformed Eq. (17) into Eq. (24). We now perform a similar analysis on the dimensionless half-width $B^*$of the cross section. The power index N is isolated by rearranging Eq. (15) as follows:

$$B^* S^{*-1} \propto (S^{*1/3} U^{*-1})^N \tag{27}$$

Fig. 10 plots $B^* S^{*-1}$ versus $S^{*1/3} U^{*-1}$ computed from the measurements. The half-widths at the lower and upper sides of the trajectory were not discriminated in the present experiment, as their values were similar. The power index N was evaluated as 0.004, indicating that $B^* S^{*-1}$ and $S^{*1/3} U^{*-1}$ are essentially independent. This result is consistent with that of the dimensionless temperature elevation T^* along the trajectory, obtained in the previous subsection. However, note again that we cannot conclude a negligible effect of the cross-wind velocity U^* on the dimensionless half-width of the cross section B^*; rather, the effect can be consolidated into the dimensionless distance S^* along the trajectory, as the trajectory is bent by the cross-wind.

Assuming that the power index N is zero, the dimensionless half-width of the cross section B^* was correlated with the dimensionless distance along the trajectory S^*. The results are shown in Fig. 11. Although the data points are somewhat scattered, they are clearly correlated and satisfy the following two-parameter regression equation:

$$B^* = 0.300 S^* + 0.0445 \quad (R^2 = 0.755) \tag{28}$$

Like the dimensionless temperature elevation T^* along the trajectory, this equation is satisfied in a quiescent environment. As an example, we add the equivalent result of Zukoski et al. [22] given by,

$$B^* = 0.131 S^* \tag{29}$$

to Fig. 11. The proportionality coefficient was 0.300 in the present experiment, versus 0.131 in the quiescent environment [22]. The magnitude relationship of the coefficient, the one in the cross-wind environment is greater than the one in a quiescent environment, is consistent with the previous discussion that the entrainment rate of ambient air into fire plumes is greater in the cross-wind environment.

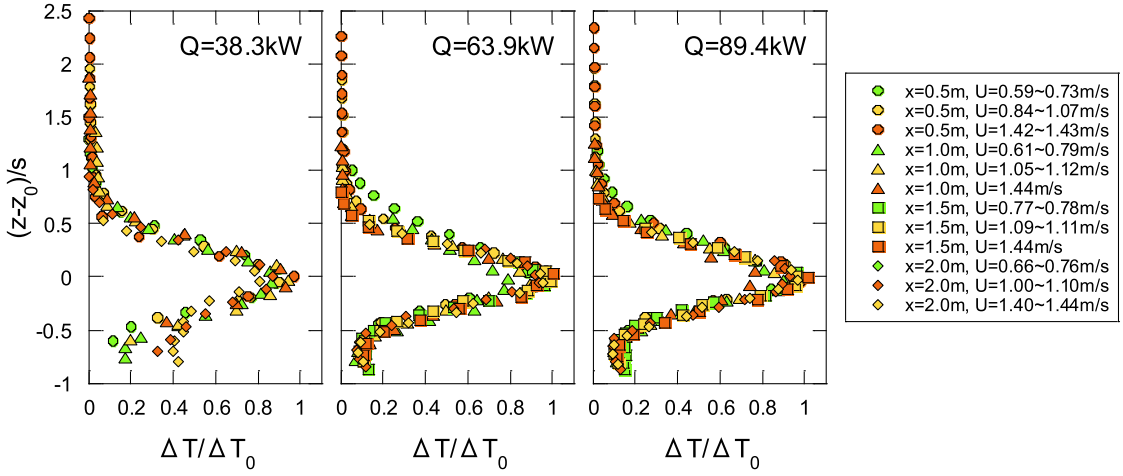

Fig. 9. Normalized temperature elevation versus normalized separation from the trajectory in fire plumes with different heat release rates and cross-wind velocities.

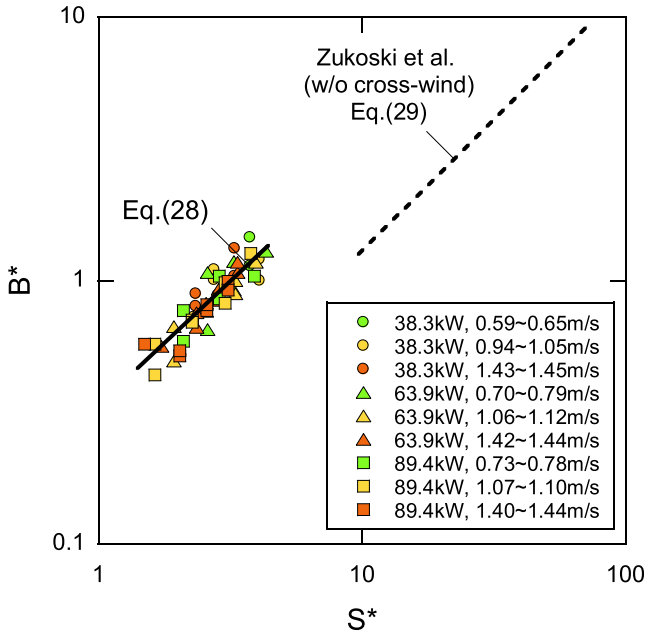

Fig. 11. Dimensionless half-width of the cross section along the trajectory of a fire plume.

4.4. Ground-level temperature elevation

For maintaining the safety of human activity around large outdoor fires, the ground-level temperature elevation is often more important than the temperature elevation along the trajectory. Thus, Fig. 12 plots the change in temperature elevation ΔT at 0.02 m above the floor (the ground-level temperature elevation) versus distance from the flume source in the wind direction (x-direction) for a number of test cases. In contrast with the temperature elevation along the trajectory (Fig. 6), the distribution of data points implies that the cross-wind velocity U_∞ significantly affects the ground-level temperature elevation ΔT. Especially, ΔT increases with increasing U_∞ for fire plumes with the same heat release rate $\dot{Q}$. Also note that date points include ΔT in the continuous flame and intermittent flame regions depending on U_∞ and $\dot{Q}$, since the thermocouples were aligned close to fire sources for the ground-level measurement.

As shown in the previous subsection, the dimensionless temperature elevation along the trajectory was well correlated with the dimensionless distance along the trajectory S^*. Accordingly, Fig. 13 plots the dimensionless ground-level temperature elevation T^* against the dimensionless horizontal distance X^*. Although there is a rough trend in the distribution, the data points are quite variable because no parameter represents the cross-wind effect in this correlation (recall that in the temperature elevation along the trajectory, the cross-wind effect was embodied in the distance along the curved trajectory).

To improve the correlations in the experimental data, we introduce a virtual point source that adjusts for the effects of fire size and cross-wind [23]. As the adjustment function, we obtained an expression that approximates the overall distribution of the data points:

$$T^* = \begin{cases} 2.73 & (X^* < 0.358) \\ 0.35X^{*-2} & (0.358 \le X^* < 1.0) \\ 0.35X^{*-5/3} & (1.0 \le X^*) \end{cases} \quad (30)$$

where X^* is a dimensionless parameter given by

$$X^* = \frac{x}{D} = x/\left(\frac{\dot{Q}}{c_P \rho_\infty T_\infty g^{1/2}}\right)^{2/5} \quad (31)$$

Dimensionless temperature elevation T^* was split into three parts considering that the data points include those in the continuous flame and intermittent flame regions in addition to those in the plume region. However, the threshold values are not based on any experimental observation, but they are chosen through trial and error so that the expression well approximates the data points. The power index for $1.0 \le X^*$ was taken from Eq. (17), though the others were determined empirically. The separation ΔX^* of a data point from Eq. (30) in the X^*-direction defines the degree that requires adjustment. The parameter generalizing the separations ΔX^* is selected somewhat arbitrarily. Here we take the product of the dimensionless heat release rate $\dot{Q}_W^*$ and the dimensionless cross-wind velocity U_W^* defined in Eq. (22). The separations ΔX^* are correlated with the dimensionless parameter $\dot{Q}_W^* U_W^*$ in Fig. 14. The data points are consistently distributed downward to the right, indicating that the virtual point source needs to be positioned further downwind as one or both of $\dot{Q}_W^*$ and U_W^* increase. In other words, as $\dot{Q}_W^*$ and U_W^* increase, the point-source concept raises the dimensionless ground-level temperature elevation T^*. The regression curve is the following logarithmic function:

$$\Delta X^* = \frac{\Delta x}{D} = -0.160\ln(\dot{Q}_W^* U_W^*) - 0.288 \quad (R^2 = 0.873) \quad (32)$$

Fig. 15 displays the updated dimensionless ground-level temperature elevation T^* versus the product of $\dot{Q}_W^*$ and U_W^*. The correlation of the data points was substantially improved by the point-source adjustment (cf. Fig. 13). Note that the dimensionless parameter X^* (equivalent to S^*) used to generalize the ground-level temperature elevation T^* was originally derived from the physical relationship in the region far downstream of fire sources. However, the dimensionless parameter was still valid in correlating T^* in the region close to fire sources where the thermocouples were even immersed in the continuous flame or intermittent flame regions.

5. Conclusion

This study derived a similarity model of temperature elevation caused by wind-blown fire plumes in relatively far downwind regions of the fire source. The model was validated against the measured results of wind tunnel experiments. One of the applications of this model is to incorporate it into physics-based urban fire spread models, in which the effect of wind-blown fire plumes on firefighting activity and evacuation of residents in the downwind region of fire sources is simulated

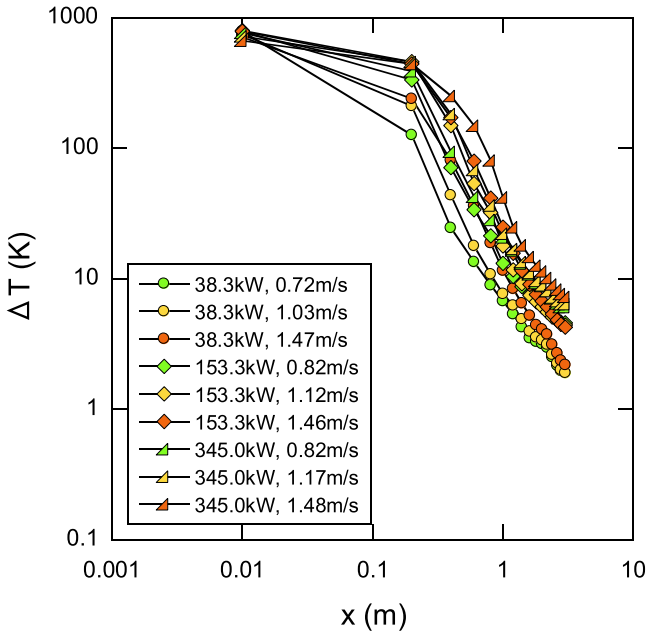

Fig. 12. Temperature elevation at 0.02 m above the floor in the downwind region of fire plumes with different heat release rates and cross-wind velocities.

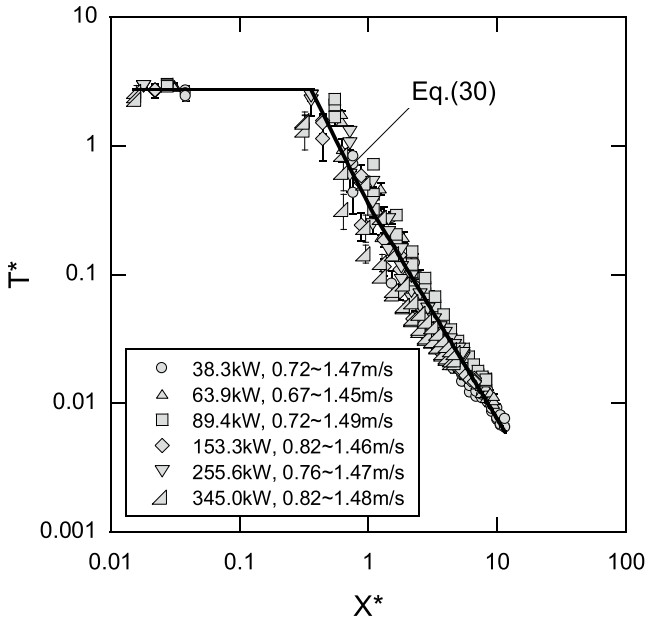

Fig. 13. Log–log plot of dimensionless ground-level temperature elevation by fire plumes with different heat release rates and cross-wind velocities, without a virtual source adjustment.

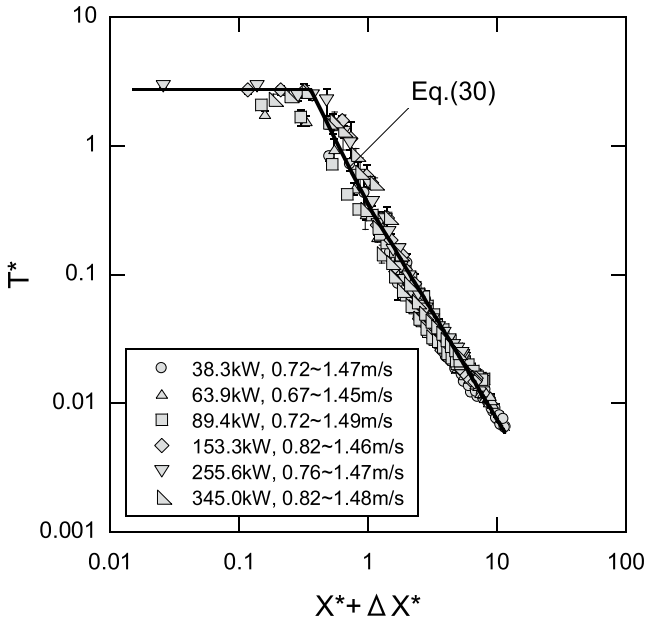

Fig. 15. Log–log plot of dimensionless ground-level temperature elevation by fire plumes with different heat release rates and cross-wind velocities, after virtual source adjustment.

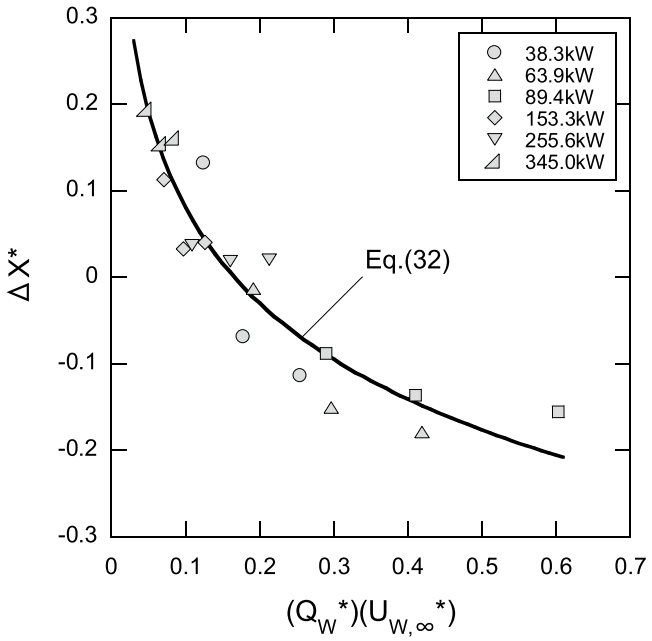

Fig. 14. Virtual point-source adjustment of horizontal distance from the fire source.

[24–26]. Reasonable degree of accuracy relative to simple calculation procedure, one of the features of similarity models, is especially advantageous in simultaneously simulating burning behavior of numerous buildings in wide-range area.

The study results are summarized below.

- A trajectory model was derived, in which the vertically upward momentum was provided by buoyancy and the horizontal velocity was equivalent to the cross-wind velocity. Although this model ignored the attenuation of vertical momentum by viscous forces, it reasonably agreed with the experimental results in the investigated parameter ranges.
- A model describing the transition of temperature elevation and cross-sectional half-width along the trajectory was derived through dimensional analysis. The derived model, which embodies the cross-wind effect in the distance along the curved trajectory, is equivalent to that in a quiescent environment. However, as revealed by the proportionality coefficients, the temperature elevation is lower and the cross-sectional half-width is considerably larger than in a quiescent environment.
- The derived model was less successful at predicting the ground-level temperature elevation. The data points were roughly correlated, but the agreement was improved by introducing a virtual point source as a function of the dimensionless heat release rate and the dimensionless cross-wind velocity.

Acknowledgement

This study was supported by JSPS KAKENHI Grant Number JP17H03369.

References

[1] P.H. Thomas, The size of flames from natural fires, Symposium (International) on Combustion, vol. 9, 1963, pp. 844–859.
[2] A.A. Putnam, A model study of wind-blown free-burning fires, Symposium (International) on Combustion, vol. 10, 1965, pp. 1039–1046.
[3] J.R. Welker, C.M. Sliepcevich, Bending of wind-blown flames from liquid pools, Fire Technol. 2 (1966) 127–135.
[4] J.R. Welker, C.M. Sliepcevich, Burning rates and heat transfer from wind-blown flames, Fire Technol. 2 (1966) 211–218.
[5] F.A. Albini, A Model for the wind-blown flame from a line fire, Combust. Flame 43 (1981) 155–174.
[6] Y. Oka, O. Sugawa, T. Imamura, Y. Matsubara, Effect of cross-winds to apparent flame height and tilt angle from several kinds of fire source, Fire Saf. Sci. 7 (2003) 915–926.
[7] L. Hu, S. Liu, J.L. de Ris, L. Wu, A new mathematical quantification of wind-blown flame tilt-angle of hydrocarbon pool fires with a new global correlation model, Fuel 106 (2013) 730–736.
[8] L. Hu, L. Wu, S. Liu, Flame Length Elongation Behavior of Medium Hydrocarbon Pool Fires in Cross Air Flow, 111 2013, pp. 613–620.
[9] L. Hu, A review of physics and correlations of pool fire behavior in wind and future challenges, Fire Saf. J. 91 (2017) 41–55.
[10] Y. Lin, X. Zhang, L. Hu, An experimental study and analysis on maximum horizontal extents of buoyant turbulent diffusion flames subject to relative strong cross flows, Fuel 234 (2018) 508–515.
[11] S. Yokoi, Temperature distribution downwind of the line heat source, Bulletin of Japan Association for Fire Science and Engineering 13 (1965) 49–55.

[12] T. Saga, Temperature distribution of fire gas flow from a belt-shaped heat source under strong wind, Journal of Structural and Construction Engineering 408 (1990) 99–110.
[13] Y. Hayashi, T. Saga, Experimental study on temperature distributions in fire-induced flows, Journal of Architecture and Planning 566 (2003) 25–32.
[14] Y. Oka, O. Sugawa, T. Imamura, Y. Takeishi, M. Honma, Modeling on the trajectory of an inclined fire plume in cross-winds, Bulleting of Japan Association for Fire Science and Engineering 55 (2005) 49–56.
[15] Y. Oka, O. Sugawa, T. Imamura, Correlation of temperature rise and velocity along an inclined fire plume axis in crosswinds, Fire Saf. J. 43 (2008) 391–400.
[16] J. Counihan, An improved method of simulating an atmospheric boundary layer in a wind tunnel, Atmos. Environ. 3 (1969) 197–214.
[17] N.J. Cook, Wind-tunnel simulation of the adiabatic atmospheric boundary layer by roughness, barrier and mixing device methods, J. Ind. Aerodyn. 3 (1978) 157–176.
[18] H.P.A.H. Irwin, The design of spires for wind simulation, J. Wind Eng. Ind. Aerod. 7 (1981) 361–366.
[19] J. Counihan, Adiabatic atmospheric boundary layers: a review and analysis of data from period 1880-1972, Atmos. Environ. 9 (1975) 871–905.
[20] Architectural Institute of Japan, Recommendations for Loads on Buildings, fourth ed., Maruzen, 2015.
[21] B.R. Morton, G. Taylor, J.S. Turner, Turbulent gravitational convection from maintained and instantaneous sources, Proceedings of Royal Society 234A (1956) 1–23.
[22] E.E. Zukoski, T. Kubota, B.M. Cetegen, Entrainment in fire plumes, Fire Saf. J. 3 (1981) 107–121.
[23] G. Heskestad, Virtual origin of fire plumes, Fire Saf. J. 5 (1983) 109–114.
[24] K. Himoto, T. Tanaka, Development and validation of a physics-based urban fire spread model, Fire Saf. J. 43 (2008) 477–494.
[25] K. Himoto, K. Mukaibo, R. Kuroda, Y. Akimoto, A. Hokugo, T. Tanaka, A post-earthquake fire spread model considering damage of building components due to seismic motion and heating of fire, Fire Saf. Sci. 10 (2011) 1319–1330.
[26] K. Himoto, T. Tanaka, A model for the fire-fighting activity of local residents in urban fires, Fire Saf. J. 54 (2012) 154–166.